*Research Article*

# Synthesis and Characterization of Poly(urethane-ether azomethine) Fatty Amide Based Corrosion Resistant Coatings from *Pongamia glabra* Oil: An Eco-Friendly Approach

**Manawwer Alam,[1] Naser M. Alandis,[2] Naushad Ahmad,[2] and Mu Naushad[2]**

[1]*Research Center, College of Science, King Saud University, P.O. Box 2455, Riyadh 11451, Saudi Arabia*
[2]*Department of Chemistry, College of Science, King Saud University, P.O. Box 2455, Riyadh 11451, Saudi Arabia*

Correspondence should be addressed to Manawwer Alam; malamiitd@gmail.com

Academic Editor: Carola Esposito Corcione

A novel attempt has been made to incorporate azomethine group in the backbone of polyurethane ether *Pongamia* oil fatty amide. The overall reaction was carried out in different steps like preparation of N,N-bis(2-hydroxyethyl) *Pongamia glabra* oil fatty amide, poly(ether fatty amide), and poly(urethane-ether) fatty amide. The hydroxyl terminated Schiff base, ethane 1,2-di(azomethine) bisphenol, reacts with fatty amide diol and is further treated with toluylene 2,4-diisocynate (TDI) to form poly(urethane-ether azomethine) fatty amide (PUEAF). These synthesized resins were characterized by FT IR, $^1$H NMR, and $^{13}$C NMR spectroscopic techniques. Molecular weight of PUEAF resin was measured by gel permeation chromatography (GPC), coating was made on mild steel strips, and evaluating their physicochemical and physicomechanical analysis was carried out by standard methods. The PUEAF25 coating showed highest scratch hardness (2.5 kg), gloss (90) at 45°, pencil hardness (4H), and impact resistance (150 lb/inch). Atomic force microscopy (AFM) and differential scanning calorimetry (DSC)/thermogravimetric analysis (TGA) were used to determine the topography and thermal behavior of PUEAF. Corrosion studies of PUEAF coated mild steel were used in different corrosive media (3.5 wt% HCl, 5 wt% NaCl, and tap water) at room temperature using potentiodynamic polarization technique. The results of this study showed that PUEAF coatings exhibit good physicomechanical, anticorrosive properties and get application up to 180°C.

## 1. Introduction

Organic coatings are widely used for protection of mild steel against corrodents and to provide aesthetic appeal. Various types of polymeric organic coatings from different renewable resources like lignin, cellulose, vegetable oils [VO], and others are used to protect mild steel [1–4]. To further improve coating performance, inorganic moieties are incorporated into organic polymer coatings yielding hybrids [5, 6]. Hybrid coatings show excellent mechanical properties, hardness, wear resistance, and chemical stability against solar radiations and pollutants in atmosphere [7], often good hydrophobicity [8], and transparency [9]. Hybrid coatings have also shown antibacterial and antifungal behavior [10].

VO are one of the most important renewable resources for production of polymeric materials like alkyd, polyesteramide,

polyetheramide, polyurethane, polyester, polyepoxy, and polyamine amide in combination with commercial polymers such as polyvinyl alcohol, polystyrene, polymethylmethacrylate, and polyurethane [11–15]. VO such as linseed, *Pongamia*, olive, castor, *Jatropha*, soybean, *Mesua ferrea*, cotton seed, neem (*Azadirachta indica*), tung, corn, and *Annona squamosa* are used for the production of polymeric coatings [16–23]. The utilization of VO has attracted great attention in both scientific and industrial applications due to easy availability, environmental friendliness, low volatile organic matter, and cost-effectiveness [24–27].

Schiff base (azomethine) also called imine (-C=N-) has nitrogen; it is basic and exhibits pi-acceptor properties. Imine group possesses excellent donor properties and is used as ligands, enzymatic intermediates in coordination chemistry

and biochemistry, respectively. Schiff base compounds are corrosion resistant antimicrobial with good thermal properties [28, 29]. The main drawbacks of Schiff base polymers are brittleness and lack of toughness [30–32]. Keeping in mind these properties, we introduced azomethine group in oil fatty amide through ether linkage and further modified by urethane. Thus, the approach is synergistic benefitting both the constituents and rendering a corrosion resistant coating material.

The goal of present study is the development of new poly(urethane-ether azomethine) fatty amide (PUEAF) hybrid from seed oil of *Pongamia glabra*, by the introduction of inorganic Schiff base moiety. The synthesis of PUEAF hybrid is divided into four steps: (i) synthesis of ethane 1,2-di(azomethine) bisphenol (EAB), (ii) synthesis of N,N-bis(2-hydroxyethyl) *Pongamia glabra* oil fatty amide (HEFA), (iii) synthesis of poly(ether azomethine) fatty amide (PEAF), and (iv) synthesis of poly(urethane-ether azomethine) fatty amide (PUEAF). The products obtained in each step were characterized by FT IR, ^{1}H NMR, and ^{13}C NMR spectroscopy. The physicochemical characterization of PUEAF resin was carried out by standard methods. PUEAF were applied as coatings on mild steel panels for physicomechanical analysis. The thermal stability of PUEAF resins was investigated by thermogravimetric analysis (TGA) and differential scanning calorimetry (DSC). The corrosion resistance performance of PUEAF was investigated by potentiodynamic polarization measurements at ambient temperature.

## 2. Materials and Methods

*2.1. Materials.* *Pongamia glabra* oil was extracted from seeds through Soxhlet apparatus using petroleum ether (BP 60–80°C) and characterized by Gas Liquid Chromatography (Perkin Elmer Model 716, USA) with FID detector [19, 33]. Diethanolamine (Riedel-de Haen, Germany), petroleum ether, sodium methoxide, methanol, xylene, ethylene diamine (BDH Chemicals, Ltd., Poole, England), 4-hydroxybenzaldehyde (Koch-Light Laboratories, Coinbrook Bucks, England), and toluylene 2,4-diisocynate (Acros Organic, USA) were used as received. Mild steel panels (99.51% Fe, 0.34% Mn, 0.10% C, and 0.05% P) were purchased from Fancy Steel Company, Tianjin, China.

*2.2. Synthesis of Ethane 1,2-Di(azomethine) Bisphenol (EAB).* 4-Hydroxybenzaldehyde (2.44 g, 0.02 mol) was dissolved in 50 mL of methanol and ethylene diamine (0.60 g, 0.01 mol) was added. The reaction mixture was refluxed for 6 hours at 60°C with continuous stirring. The colour of solutions changed from wine red to dark red after addition of ethylene diamine. The reaction was monitored by TLC. After completion of reaction, methanol was removed through vacuum evaporator and distilled water was added to obtain precipitate of EAB. EAB was washed with diethyl ether several times and dried in vacuum oven.

*2.3. Synthesis of N,N-Bis(2-hydroxyethyl) Pongamia glabra Oil Fatty Amide (HEFA).* HEFA was synthesized according to previously reported method [17, 34].

*2.4. Synthesis of Poly(ether azomethine fatty amide) (PEAF).* HEFA (3.60 g), EAB (2.50 g), and 100 mL xylene were taken in a four-necked conical flask with Dean Stark trap, thermometer, nitrogen inlet, and stirrer and heated up to 180°C, for 2 h under continuous stirring. The procedure followed was according to our earlier reported paper [17].

*2.5. Synthesis of Poly(urethane-ether azomethine fatty amide) (PUEAF).* PEAF and TDI (20, 25, 30 wt%) along with xylene were placed in four-necked conical flask fitted with condenser, nitrogen inlet, thermometer, and stirrer. The reaction was carried out under stirring at 120°C, till the completion of the reaction.

*2.6. Methods.* HEFA, PEAF, and PUEAF resins were evaluated by spectroscopic techniques such as FT IR, ^{1}H NMR, and ^{13}C NMR. FT IR spectra of HEFA, PEAF, and PUEAF resins were taken on FT IR spectrometer, Spectrum 100, Perkin Elmer, USA. ^{1}H and ^{13}C NMR spectrum were recorded on Jeol DPX 400 MHz using deuterated chloroform/dimethyl sulphoxide as solvents and tetramethylsilane as an internal standard. Thermal analysis of PUEAF resin was carried out by thermogravimetric analysis (TGA) and differential scanning calorimetry (DSC) (Model TGA/DSC 1, Mettler Toledo AG, Analytical CH-8603, Schwerzenbach, Switzerland) in nitrogen atmosphere, from 40°C to 350°C for DSC and from 25°C to 800°C for TGA with heating rate of 10°C/min. Molecular weight (Mw and Mn) of PUEAF resin was investigated by GPC (HT-GPC Module 350 A, Viscotek, Houston, TX, USA). THF was used as eluent at a flow rate 1.0 mL/min and instrument was calibrated with polystyrene standard. Topography of PUEAF coated panels was measured by Atomic Force Microscope (AFM) in noncontact mode, Model TriA SPM, APE Research, s.r.l. Area Science Park, Basovizza 34149, Trieste, Italy. AFM was equipped with a piezoelectric scanner and HQ:CSC17 Cantilevers (Mikro Masch D35578, Wetzlar, Germany). Cantilevers have been used with Cr-Au/Pt coated tip, length $450 \pm 5\,\mu m$, width $50 \pm 3\,\mu m$, thickness $2.0 \pm 0.5\,\mu m$, force constant 0.06–0.40 N/m, and resonance frequency 10–17 kHz.

*2.7. Preparation and Testing of Coatings.* 40% solutions of PUEAF resins in xylene were applied by dip method on commercial mild steel strips with standard sizes (70 × 25 × 1 mm) for analysis, cured at ambient temperature and atmosphere. The PUEAF coating curing occurred by evaporation of solvent, reaction free isocynates with moisture, and autooxidation. PUEAF coated strips were tested for impact resistance (IS: 101 part 5/sec 3, 1988), scratch hardness (BS 3900), and salt spray test (ASTM D1654). Thickness of coatings was measured by Elcometer Coating Thickness Gauge (Model 456; Elcometer Instruments, Manchester, UK). Gloss of coatings was measured by gloss meter (Model RSPT20; digital instruments, Santa Barba, CA, USA). Adhesion test was carried out (ASTM D3359-02) by cross hatch adhesion tester consisting of 11 with 1 mm spacing of blades. The test was carried out by pressing and passing the adhesion tester on coated panel into two directions at right angle to each other. The square adhesive tape was adhered over panel and after 5

minutes removed sharply. The adhesion of film was measured from number of squares detached with tape. The results were obtained by comparing number of squares detached by peeling off the adhesive tape with number of squares that stayed on sheets. In *flexibility test*, the coated mild steel strips were bent, this tested ability of coating to resist cracking when elongated. Flexibility of coated panels was verified on a conical mandrel tester (ASTM D3281-84). While performing assessment, the mandrel was free to rotate on its axis, and then coated samples were kept in between revolving axes. The lever of conical mandrel was lowered in a perpendicular direction to obtain specific angles. The pencil hardness of coated panel was observed by pencil hardness tester (Wolff-Wilborn Tester, Sheen Instruments, England). In this test, pencils having different types (9B, 8B, 7B, 6B, 5B, 4B, 3B, 2B, B, HB, F, H, 2H, 3H, 4H, 5H, 6H, 7H, 8H, and 9H) from softer (darker) to hard (lighter) grade were used to move over surface of coated panel from a distance of 6 mm at fixed angle (45°) by using standard holder. Force (7.5 N) was applied to the pencil, moving it over surface of examination of the panel, at fixed angle. The coated panels were checked for scratches on the film. The same process was repeated with pencil of upper grade of hardness as long as film was not scratched. The pencil hardness of the coating corresponds to the highest degree of hardness which the coating resists without being scratched.

Corrosion resistance studies of PUEAF coated mild steel strips were accomplished using Gill AC (ACM Instruments, Cumbria, England, UK). The inhibition efficiency of different PUEAF coated panels was evaluated in relation to bare mild steel. For this study potentiodynamic polarization curves were prepared by polarizing the working electrode at ±250 mV in relation to corrosion potential at a scanning rate of 5 mV/s. The exposed surface area of working electrode was 1 cm$^2$ in 250 mL volume of solution. The electrochemical circuit was completed with platinum counter electrode and calomel reference electrode. Polarization resistance, corrosion current, corrosion potential (open circuit potential), and Tafel constant ($B_a$, $B_c$) values curve were calculated by extrapolating the linear portion of the curve. All measurements were accomplished in triplicate form in different corrosive media like 3.5% HCl, 5.0% NaCl, and tap water (Cl$^-$ ion 164 ppm) [5].

## 3. Results and Discussion

Schemes 1, 2, and 3 show synthesis of EAB, PEAF, and PUEAF, respectively. EAB was synthesized by chemical reaction between 4-hydroxybenzaldehyde and ethylene diamine. Synthesis of PEAF was carried out from the reaction of HEPA with EAB and further treated with TDI to form PUEAF hybrids. The chemical reactions were ascertained with help of FT IR, $^1$H NMR, and $^{13}$C NMR spectroscopy.

### 3.1. Spectral Analysis

*EAB. FT IR (KBr, cm$^{-1}$)*: 3456 (OH); 2938 (-CH$_2$- asymmetrical); 2854 (-CH$_2$- symmetrical); 1628 (-CH=N-); 1278 (-O-Ar); 778, 790 (aromatic ring). *$^1$H NMR (DMSO-d$_6$, δ*
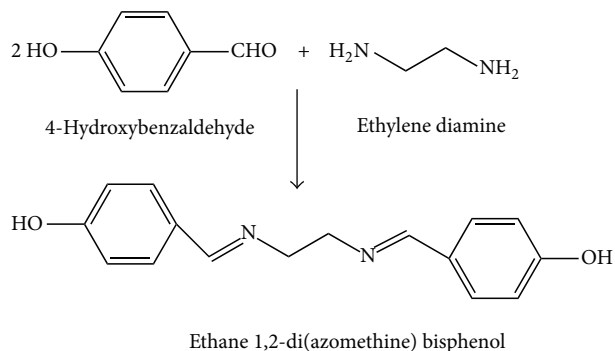


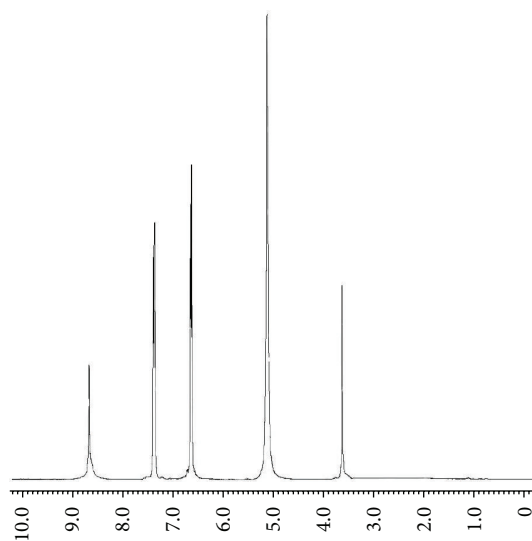Scheme 1: Synthesis of ethane 1,2-di(azomethine) bisphenol (EAB).
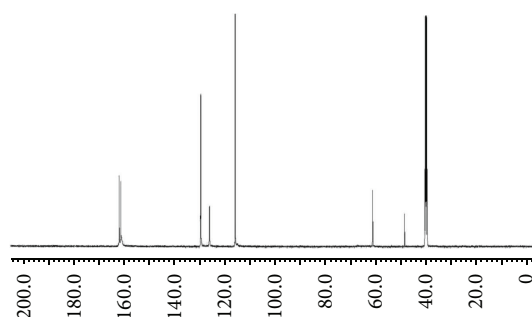


Figure 1: $^1$H NMR spectra of EAB.



Figure 2: $^{13}$C NMR spectra of EAB.

*ppm)*: 5.351 (-**O**H); 8.742 (-**C**H=N-, azomethine); 6.850–7.781, (-**C**H-, aromatic); 3.003 (-**C**H$_2$-, aliphatic) (Figure 1). *$^{13}$C NMR (DMSO-d$_6$, δ ppm)*: 161.159 (-**C**H=N-); 115.508, 126.672, 129.567 (-**C**H-, aromatic); 61.652 (-**C**H$_2$- aliphatic) (Figure 2), melting point 148°C.

*PEAF. FT IR (cm$^{-1}$)*: 3454 (OH); 2953 (-CH$_2$- asymmetrical); 2854 (-CH$_2$- symmetrical); 3007 (-CH=CH-); 1628 (-CH=N-); 1617 (C=O, amide); 1461 (C-N, amide); 1278 (-O-Ar); 1520, 1464, 771, 734 (aromatic ring). *$^1$H NMR (CDCl$_3$,*
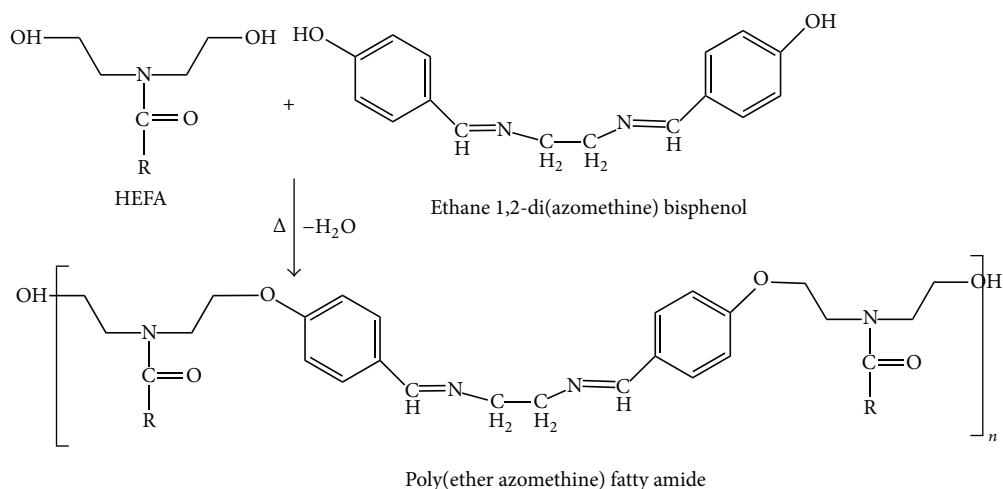
Scheme 2: Synthesis of PEAF.
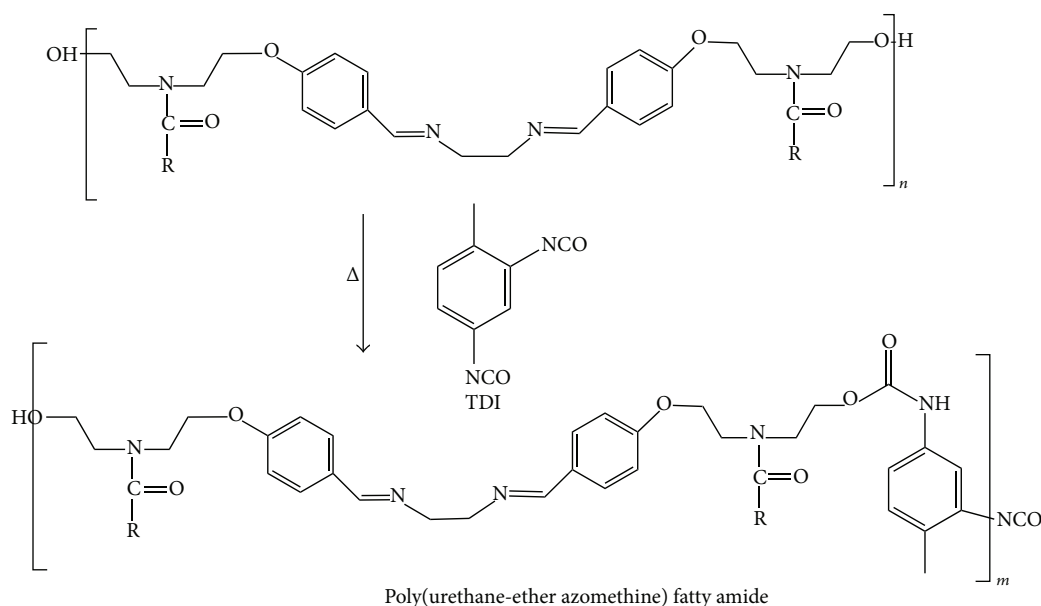


Scheme 3: Synthesis of PUEAF.

$\delta$ ppm): 0.825–0.860 (-CH$_3$); 1.217–1.265 (-CH$_2$-); 1.965–2.001 (-CH$_2$-, attached double bond); 2.310 (CH$_2$ between double bond); 2.780 (CH$_2$ attached to amide CO) 3.523–3.570 (-CH$_2$OH); 3.728–3.741 (-CH$_2$- attached amide nitrogen); 4.164 (-CH$_2$ attached O); 4.702 (-CH$_2$OH); 5.291–5.305 (-CH=CH-); 6.82–6.84, 7.528 (aromatic ring); 8.713 (CH=N, azomethine) (Figure 3). $^{13}$C NMR (CDCl$_3$, $\delta$ ppm): 14.066 (-CH$_3$); 22.630–29.719 (-CH$_2$-); 31.852 (-CH$_2$ attached amide carbonyl); 54.096 (-CH$_2$- attached to nitrogen); 63.451 (-CH$_2$ attached to O); 115.131, 129.954, 154.976 (aromatic ring); 163.652 (-CH=N-); 176.453 (C=O, amide) (Figure 4).

PUEAF. FT IR (cm$^{-1}$): 3320 (OH); 2958 (-CH$_2$- asymmetrical); 2856 (-CH$_2$- symmetrical); 3010 (-CH=CH-); 2270 (-NCO free), 1625 (-CH=N-); 1615 (C=O, amide); 1466 (C-N, amide); 1711 (NH, urethane); 1270 (-O-Ar); 1526, 1466, 775, 742 (aromatic ring). $^1$H NMR (CDCl$_3$, $\delta$ ppm): 0.817–0.868 (-CH$_3$); 1.237–1.276 (-CH$_2$-); 1.955–2.101 (-CH$_2$-, attached double bond); 2.325 (CH$_2$ between double bond); 2.681 (CH$_2$ attached to amide CO) 3.503–3.521 (-CH$_2$OH); 3.718–3.721 (-CH$_2$- attached amide nitrogen); 4.204 (-CH$_2$ attached O); 4.682 (-CH$_2$OH); 5.301–5.325 (-CH=CH-); 6.80–6.84 (aromatic ring); 7.96 (-NH, urethane) 8.752 (CH=N, azomethine) (Figure 5). $^{13}$C NMR (CDCl$_3$, $\delta$ ppm): 14.043 (-CH$_3$); 21.239–29.658 (-CH$_2$-); 32.852 (-CH$_2$ attached amide carbonyl); 58.234 (-CH$_2$- attached to nitrogen); 64.032 (-CH$_2$ attached to O); 115.232, 129.817, 155.823 (aromatic ring); 161.582 (C=O, urethane); 164.252 (-CH=N-); 177.452 (C=O, amide) (Figure 6).
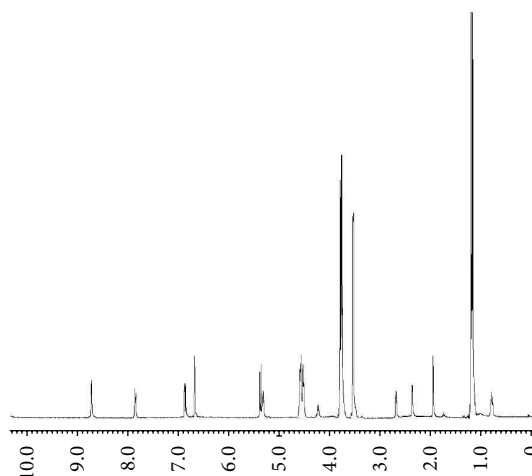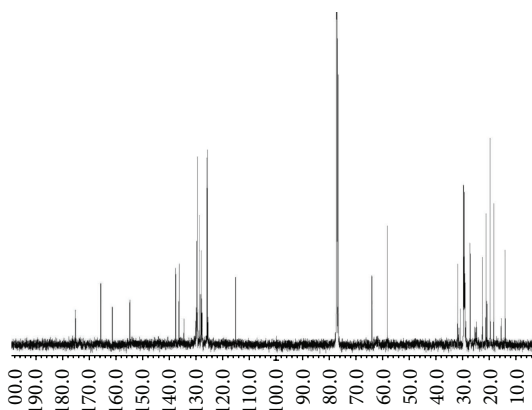
PEAF spectra show the presence of the absorption bands typical for those present in FTIR, $^1$H NMR, and $^{13}$C NMR of HEFA [17, 34]. Additional peaks appear for aromatic ring
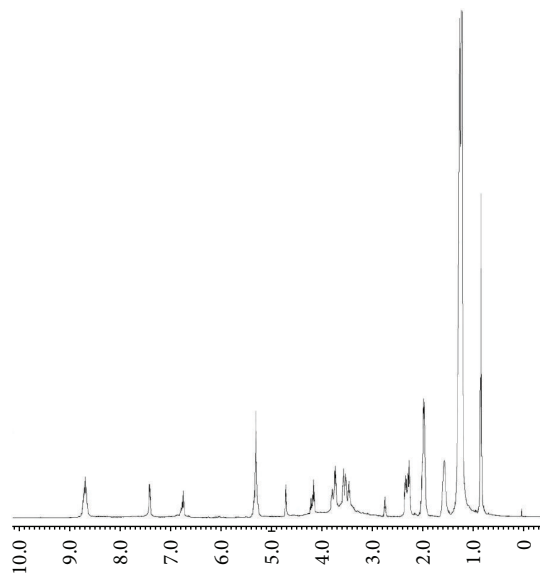
Figure 3: $^1$H NMR spectra of PEAF.
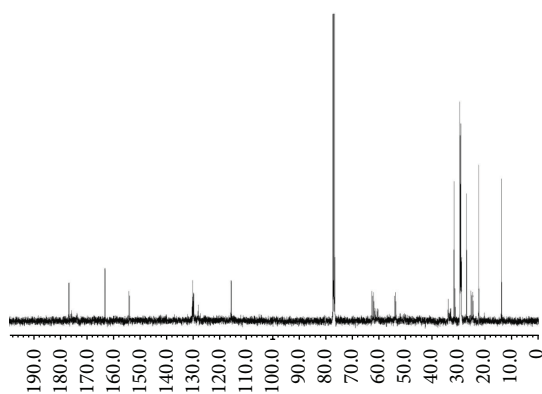


Figure 4: $^{13}$C NMR spectra of PEAF.



Figure 5: $^1$H NMR spectra of PUEAF25.



Figure 6: $^{13}$C NMR spectra of PUEAF25.

and azomethine group conferred by EAB. The absorption bands for -OH show slight depression relative to HEFA, due to consumption of -OH during the reaction.

Similarly, spectra of PUEAF show the presence of aromatic ring and azomethine group as in PEAF. Additional absorption bands occur due the presence of -NH(-C=O)-O- and free -NCO of urethane, formed by chemical reaction between free -OH of PEAF and -NCO of TDI. Molecular weight of PUEAF25 was observed to be 7267 (Mw) and 4762 (Mn) with PDI 1.526.

*3.2. Physicochemical Analysis.* The physicochemical analysis was carried out by standard methods [35]. The results indicate that hydroxyl value (HV) and iodine value (IV) decrease from HEFA (HV = 8.2, IV = 85) to PUEAF (HV = 5.1, IV = 54) and subsequently PUEAF20 (HV = 3.3, IV = 27), PUEAF25 (HV = 2.3, IV = 24), and PUEAF30 (HV = 2.0, IV = 17). These trends suggest consumption of hydroxyl value of HEFA and EAB during the condensation reaction between hydroxyl groups in presence of acid catalyst, resulting in the formation of

PEAF. During urethane formation, hydroxyl value decreases as some terminal hydroxyl group of PEAF gets consumed by the addition reaction between the hydroxyl groups and free -NCO groups of TDI. PUEAF resin was found soluble in acetylacetone, tetrahydrofuran, formamide, dimethyl formamide, benzene, ethylene glycol dimethyl ether, xylene, ethyl methyl ketone, diethyl ether, acetone, dichloromethane, ethyl acetate, toluene, and carbon tetrachloride and insoluble in acetonitrile, methanol, ethanol, and water, partially soluble in n-hexane. The solubility results of PUEAF resin can be ascribed to dense and polar nature of the resin [15].

*3.3. Physicomechanical Properties of Coating.* PUEAF coatings dried within 25–30 minutes at ambient temperature. PUEAF coatings with minor content of TDI take more time to dry as compared to higher content. This can be accredited to good affinity of -NCO groups to undergo chemical reaction with free -OH group, thus facilitating curing of PUEAF resins at room temperature. When increasing the loading of TDI, PUEAF resins attain higher cross-link density, which also accelerates fast drying at ambient temperature. The optimum cross-linking is achieved in case of 25 wt% loading of TDI in PUEAF resin, which is responsible for the shortest curing

TABLE 1: Physicomechanical characterization of PUEAF coatings.

| Resin code[*] | PUEAF20 | PUEAF25 | PUEAF30 |
|---|---|---|---|
| Gloss at 45° | 88 | 90 | 97 |
| Scratch hardness (kg) | 1.9 | 2.5 | 2.3 |
| Pencil hardness | 1H | 4H | 3H |
| Bend test (1/8 inch) | Passes | Passes | Passes |

[*]Last numeral digit indicates the loading of TDI in PUEAF resins.



FIGURE 7: Tafel plots of bare MS and PUEAF coated MS in tap water.
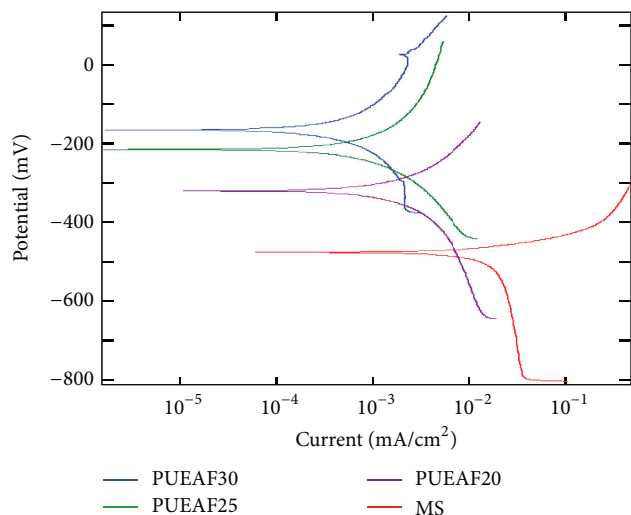


FIGURE 8: Tafel plots of bare MS and PUEAF coated MS in 5% NaCl solution.

time for PUEAF25. Thickness of coatings was found as $80 \pm 5$ microns.

Table 1 indicates that scratch hardness increases up to PUEAF25 and after that decreases as the additional NCO groups of TDI provide too much cross-linking. All the coatings passed 100% impact (150 lb/inch), bending (1/8 inch), and crosscut adhesion test, which showed good interface between substrate and coatings due to the presence of polar groups like azomethine, carbonyl, hydroxyl, and urethane in polymeric chain. PUEAF coating showed gloss values 88, 90, and 97 at 45° and passed pencil hardness maximum 4H showing good interaction between substrate and coatings.

3.4. Potentiodynamic Studies. The protective properties of PUEAF coated mild steel (MS) in different corrosive media such as tap water (72 h), NaCl (60 h), and HCl (120 h) were assessed by potentiodynamic polarization curve. The Tafel polarization curves (Figure 7) for different compositions such as PUEAF20, PUEAF25, and PUEAF30 coatings were conducted in tap water. Table 2 exemplifies the corrosion rates from bare MS to coated MS with PUEAF20, PUEAF25, and PUEAF30 and their values were $8.350E - 01$, $6.044E - 03$, $2.222E - 03$, and $1.524E - 03$ mm/y, respectively. In the case of PEAF resin, after increasing the loading of TDI such as PUEAF20, PUEAF25, and PUEAF30 corrosion rate decreases in tap water. These results indicate that PUEAF can act as a protective layer on bare MS in tap water and improve the whole anticorrosion performance. The Tafel
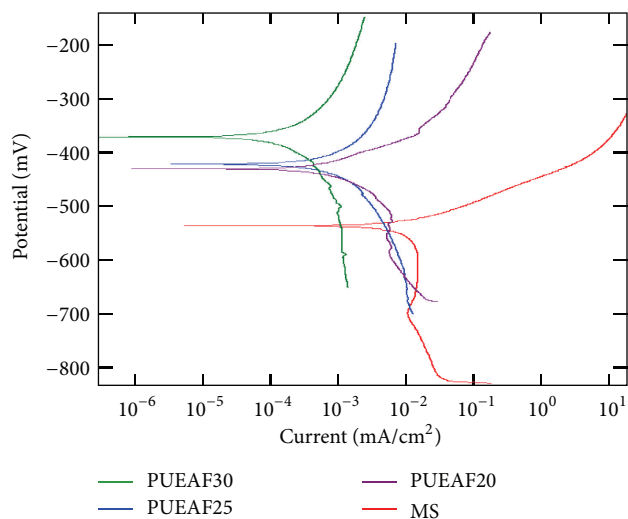
polarization curve showed that PUEAF film causes a positive displacement in the corrosion potential, relative to the value of bare MS. This positive displacement for PUEAF coating was higher than bare MS and the shift in the corrosion potential confirms the protection of metal surface. Tafel measurement evidently displays that a substantial reduction in corrosion rate occurs for PUEAF30 coated coating ($1.524E - 03$ mm/year) with respect to bare MS ($8.350E - 01$ mm/year). This reduction was due to protective effect of PUEAF film on MS. Tafel curves of PUEAF coated MS and bare MS in 5 wt% NaCl solution were shown in Figure 8 and their corrosion parameters were listed in Table 2. Corrosion current density, corrosion rate, and linear polarization resistance of PUEAF coated samples were significantly changed from bare MS to PUEAF30 coated mild steel in NaCl solution. This change could be attributed to the protection behavior of PUEAF polymer coating on MS. It suggests that corrosion protective nature of PUEAF film acts as chemical barrier to mild steel [36]. Figure 9 indicates Tafel curve in 3.5% HCl solution; PUEAF coated mild steel possesses lower corrosion potential than bare MS. From Table 2 it is clear that corrosion potential of PUEAF coated panels increases significantly and reduces the corrosion current density. These results support that PUEAF coating maybe acts as protective layer for corrosive ions on mild steel and improves the corrosion performance. The Tafel curves exhibit that PUEAF film causes a positive movement in corrosion potential compared to bare MS. Furthermore, Tafel analysis showed a substantial reduction in corrosion rate for PUEAF30 coated ($5.537E - 04$ mm/year) with respect to bare MS (11.861 mm/year). Overall, it was suggested that PUEAF30 layer would act as corrosion protection and decrease in the rate of corrosion.

The values of polarization resistance ($R_p$) were carried out using linear polarization resistance (LPR) and the results were summarized in Table 2. It was observed that higher $R_p$ values were observed in the case of coated MS when compared with bare MS. PUEAF30 coatings act as protective

TABLE 2: Corrosion parameter for PUEAF coated and bare MS in different corrosive media.

| Resin code | Medium | $E_{corr}$ (mV) | $B_a$ mV/dec | $B_c$ mV/dec | $I_{corr}$ (mA/cm$^2$) | Corrosion rate (mm/y) | LPR ($R_p$) KOhm·cm$^2$ |
|---|---|---|---|---|---|---|---|
| MS | Tap water | −478.89 | 19.894 | 37.354 | $7.166E-02$ | $8.350E-01$ | 0.0788 |
| PUEAF20 | Tap water | −323.13 | 44.111 | 49.314 | $5.215E-04$ | $6.044E-03$ | 19.412 |
| PUEAF25 | Tap water | −219.65 | 34.356 | 28.050 | $1.920E-04$ | $2.222E-03$ | 34.963 |
| PUEAF30 | Tap water | −168.25 | 41.370 | 40.320 | $1.315E-04$ | $1.524E-03$ | 67.512 |
| MS | 5.0% NaCl | −535.78 | 18.287 | 31.920 | $1.441E-01$ | 1.670 | 00.035 |
| PUEAF20 | 5.0% NaCl | −430.28 | 30.045 | 30.023 | $2.148E-03$ | $2.489E-02$ | 03.039 |
| PUEAF25 | 5.0% NaCl | −422.85 | 29.029 | 26.596 | $2.653E-04$ | $3.075E-03$ | 22.743 |
| PUEAF30 | 5.0% NaCl | −370.79 | 19.809 | 26.108 | $4.200E-05$ | $4.868E-04$ | 116.59 |
| MS | 3.5% HCl | −432.80 | 36.334 | 59.161 | 1.023 | 11.861 | 00.010 |
| PUEAF20 | 3.5% HCl | −512.70 | 39.124 | 63.157 | $2.226E-02$ | $2.618E-02$ | 00.465 |
| PUEAF25 | 3.5% HCl | −460.91 | 83.472 | 85.546 | $6.083E-03$ | $7.050E-02$ | 03.020 |
| PUEAF30 | 3.5% HCl | −325.06 | 15.634 | 25.544 | $4.777E-05$ | $5.537E-04$ | 81.561 |
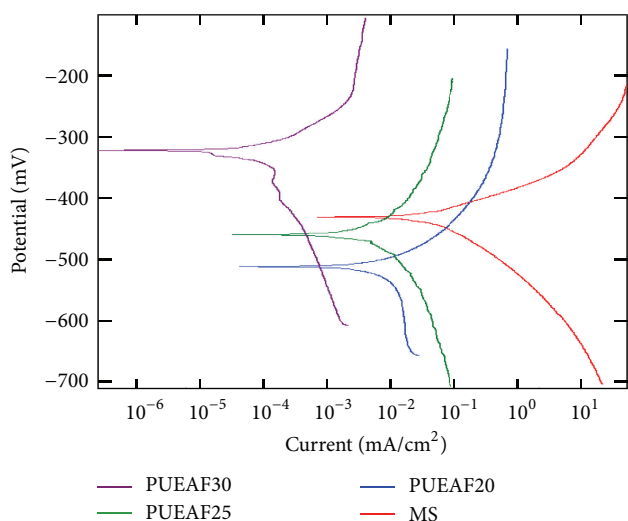


FIGURE 9: Tafel plots of bare MS and PUEAF coated MS in 3.5% HCl solution.

barrier for corrosive ions as correlated with the corrosion test performance.

*3.5. Topography Studies.* The performance of polymeric coatings is tested whether it is capable of withstanding the outer environmental effect on exposure and by examination of corrosion resistance of coatings [37], PUEAF25 coating was exposed to enhanced salt spray, to find out the defects such as pin holes and pores expected to form during curing process. Figures 10(a) and 10(b) are topographs of PUEAF25 coated sample before exposure to salt spray. It can be seen that PUEAF25 coating shows uniformity without any pin hole, indicating excellent film formation without any air trap. The percentage of rusting and blistering for PUEAF25 coated samples after 240 h of exposure in salt spray chamber was investigated. PUEAF25 coating (Figures 10(a) and 10(b)) shows that it is free from rust and blister on coating surface. A

few white spots detected indicated degradation of PUEAF25 coating matrix which is possible due to change in chemical composition of PUEAF25 coating, due to interaction with corrosive ions. AFM topography clearly informs about the surface texture of exposed PUEAF25 coating. The change in surface roughness value of exposed PUEAF25 coating shows resistance to salt spray test. A root-mean-squared (RMS) roughness of PUEAF25 coating before exposure 12.54 nm and after exposure 21.72 nm was obtained within the scanning area of 10 $\mu$m × 10 $\mu$m, while the coating with salt spray exposure is much rougher as shown in Figure 10(b). Comparison of RMS values indicates that surface texture of PUEAF25 matrix is affected after exposure to the saline environment.

*3.6. Thermal Analysis.* The TGA thermogram (Figure 11) of PUEAF coatings reveals that at initial stages loss of trapped moisture and evaporation of the entrapped solvent occur that is observed in TGA up to 350°C, which is in direct correlation with DTG, corresponding to approximately 20 wt% loss. In DSC thermogram, the same temperature range, these events can be observed as two endothermic peaks, starting from 125°C to 220°C and centered at 165°C, and another one starting from 222 to 320 centered at 270°C correlated with melting of the resins. Beyond this temperature, the ramp in TGA thermogram suggests that the sample undergoes melting followed by decomposition (the degradation of amide bond, aromatic ring, and aliphatic chain). Polyurethanes generally exhibit low thermal stability (up to 150°C) due to the presence of labile urethane groups. Here, a relatively higher thermal stability can be attributed to the formation of hybrid coatings containing azomethine group.

TGA was carried out on cured coatings of PUEAF. In DSC thermogram (Figure 12), a sharp peak indicates melting; however, here we do not observe any sharp peak; rather we observe broad endotherms, so at this temperature we cannot say that the resin is melting. The ramp in initial stages in TGA thermogram suggests that the events occurring can be the loss of moisture or entrapped solvent. The free -NCO and -NH-COO- groups in polyurethanes are very likely to
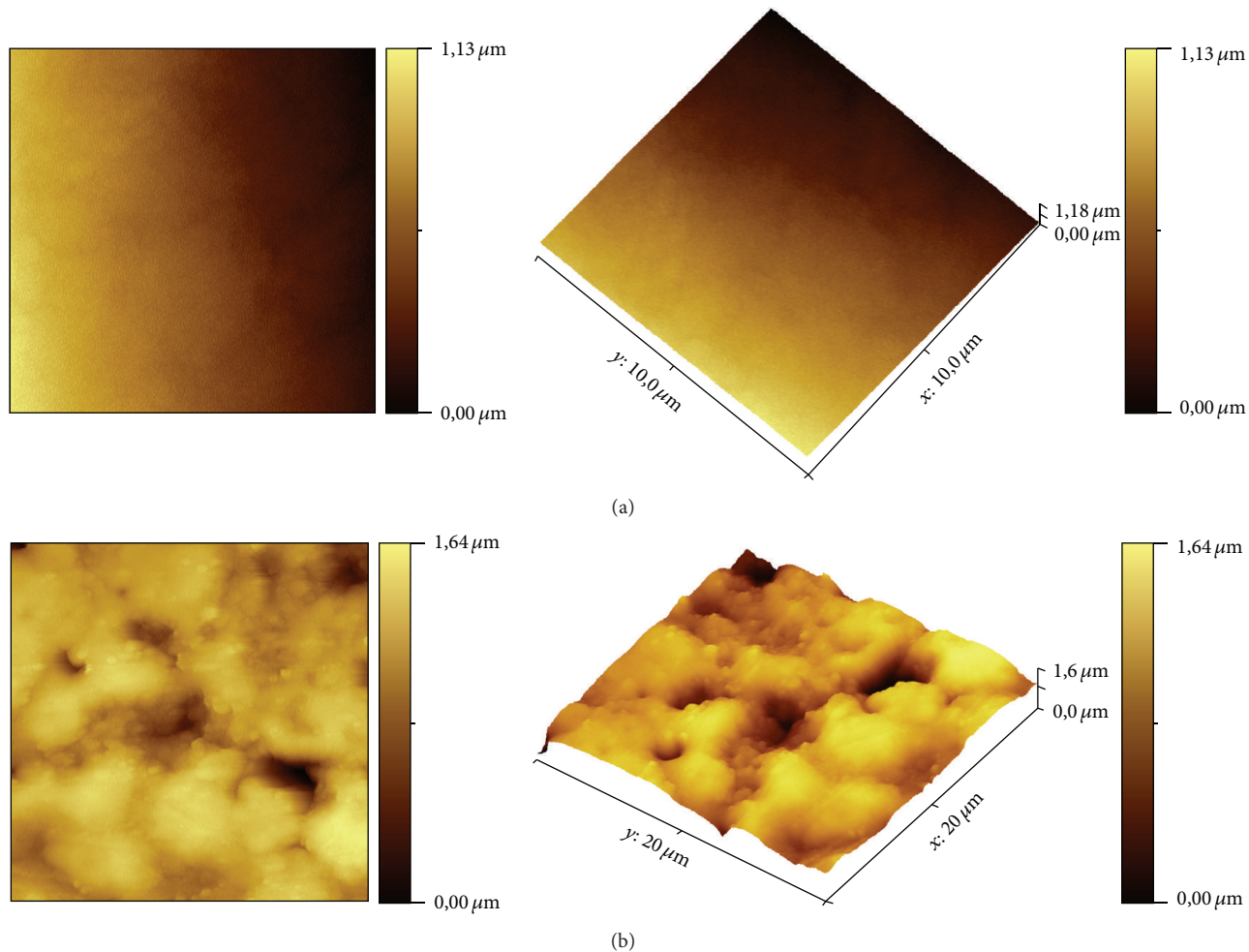
(a)



(b)

FIGURE 10: (a) AFM topographic images of unexposed PUEAF25 coating surface. (b) AFM topographic image after exposed PUEAF25 coating surface in salt spray chamber.
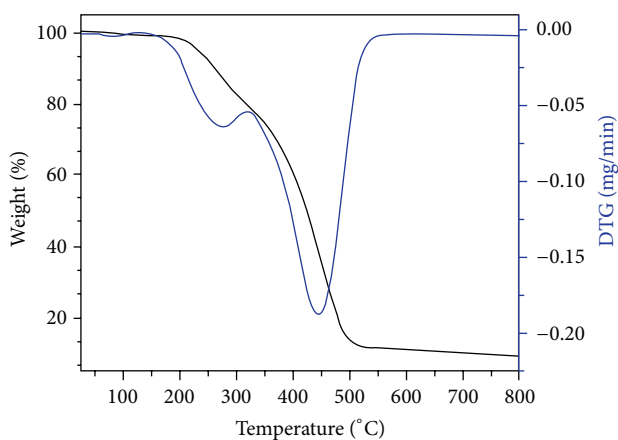


FIGURE 11: TGA/DTG thermogram of PUEAF25.



FIGURE 12: DSC thermogram of PUEAF25.

interact with moisture or even traces of water. Thus, the entrapped moisture and solvent (xylene) is expected to be evaporated at this stage in TGA thermogram. The melting
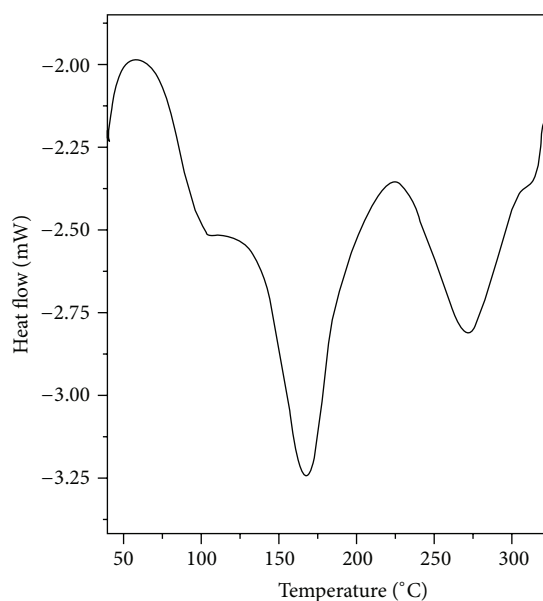
is expected to occur beyond 320°C. Thus, thermal analysis suggests that the coatings can be safely used up to 180°C.

## 4. Conclusions

Schiff base modified *Pongamia glabra* oil fatty amide diol based polyurethane exhibited an enhancement in drying properties. A unique combination of azomethine, amide, ether, and urethane in PUEAF hybrid resin improves the scratch hardness, flexibility, gloss, and anticorrosion performance. Thermal studies reveal that PUEAF25 can be safely used up to 180°C. The approach provides an alternative method for the utilization of nonedible *Pongamia glabra* oil as a corrosion protective hybrid and an environmental friendly coating material.

## Competing Interests

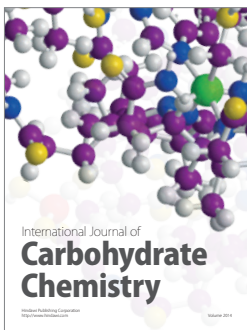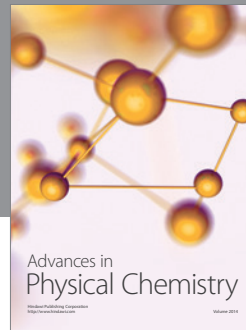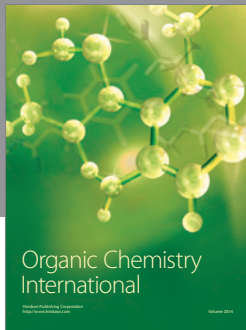The authors declare that they have no competing interests.

## Acknowledgments

## References

[1] V. Sharma and P. P. Kundu, "Condensation polymers from natural oils," *Progress in Polymer Science*, vol. 33, no. 12, pp. 1199–1215, 2008.

[2] F. S. Güner, Y. Yağcı, and A. T. Erciyes, "Polymers from triglyceride oils," *Progress in Polymer Science*, vol. 31, no. 7, pp. 633–670, 2006.

[3] M. Alam, D. Akram, E. Sharmin, F. Zafar, and S. Ahmad, "Vegetable oil based eco-friendly coating materials: a review article," *Arabian Journal of Chemistry*, vol. 7, no. 4, pp. 469–479, 2014.

[4] Y. Lu and R. C. Larock, "Novel polymeric materials from vegetable oils and vinyl monomers: preparation, properties, and applications," *ChemSusChem*, vol. 2, no. 2, pp. 136–147, 2009.

[5] C. E. Corcione, R. Striani, and M. Frigione, "UV-cured methacrylic-silica hybrids: effect of oxygen inhibition on photocuring kinetics," *Thermochimica Acta*, vol. 576, pp. 47–55, 2014.

[6] C. E. Corcione, R. Striani, and M. Frigione, "Organic-inorganic UV-cured methacrylic-based hybrids as protective coatings for different substrates," *Progress in Organic Coatings*, vol. 77, no. 6, pp. 1117–1125, 2014.

[7] C. E. Corcione, R. Striani, and M. Frigione, "Microgel modified UV-cured methacrylic-silica hybrid: synthesis and characterization," *Materials*, vol. 6, no. 9, pp. 3805–3825, 2013.

[8] C. E. Corcione, R. Striani, and M. Frigione, "Sunlight curable hybrid organic-inorganic methacrylic-based coatings: analysis of the cure mechanism and functional properties," *Polymers for Advanced Technologies*, vol. 26, no. 2, pp. 167–175, 2015.

[9] F. Graziola, F. Girardi, R. Di Maggio et al., "Three-components organic-inorganic hybrid materials as protective coatings for wood: optimisation, synthesis, and characterisation," *Progress in Organic Coatings*, vol. 74, no. 3, pp. 479–490, 2012.

[10] M. Aflori, B. Simionescu, I.-E. Bordianu et al., "Silsesquioxane-based hybrid nanocomposites with methacrylate units containing titania and/or silver nanoparticles as antibacterial/antifungal coatings for monumental stones," *Materials Science and Engineering B: Solid-State Materials for Advanced Technology*, vol. 178, no. 19, pp. 1339–1346, 2013.

[11] M. Alam and N. M. Alandis, "Corn oil based poly(ether amide urethane) coating material-synthesis, characterization and coating properties," *Industrial Crops and Products*, vol. 57, pp. 17–28, 2014.

[12] J. Argyropoulos, P. Popa, G. Spilman, D. Bhattacharjee, and W. Koonce, "Seed oil based polyester polyols for coatings," *Journal of Coatings Technology Research*, vol. 6, no. 4, pp. 501–508, 2009.

[13] M. Alam, A. R. Ray, S. M. Ashraf, and S. Ahmad, "Synthesis, characterization and performance of amine modified linseed oil fatty amide coatings," *Journal of the American Oil Chemists' Society*, vol. 86, no. 6, pp. 573–580, 2009.

[14] R. Wang and T. P. Schuman, "Vegetable oil-derived epoxy monomers and polymer blends: a comparative study with review," *eXPRESS Polymer Letters*, vol. 7, no. 3, pp. 272–292, 2013.

[15] Y. Xu, Z. Petrovic, S. Das, and G. L. Wilkes, "Morphology and properties of thermoplastic polyurethanes with dangling chains in ricinoleate-based soft segments," *Polymer*, vol. 49, no. 19, pp. 4248–4258, 2008.

[16] E. Sharmin, O. U. Rahman, F. Zafar, D. Akram, M. Alam, and S. Ahmad, "Linseed oil polyol/ZnO bionanocomposite towards mechanically robust, thermally stable, hydrophobic coatings: a novel synergistic approach utilising a sustainable resource," *RSC Advances*, vol. 5, no. 59, pp. 47928–47944, 2015.

[17] M. Alam and N. M. Alandis, "Development of poly(urethane esteramide) coatings from *Pongamia glabra* oil as anticorrosive applications," *International Journal of Polymer Analysis and Characterization*, vol. 20, no. 4, pp. 330–343, 2015.

[18] B. S. Rao and A. Palanisamy, "Photocuring and thermomechanical properties of multifunctional amide acrylate compositions derived from castor oil," *Progress in Organic Coatings*, vol. 67, no. 1, pp. 6–11, 2010.

[19] F. Zafar, H. Zafar, E. Sharmin, and S. Ahmad, "Studies on self cured zinc-containing Pongamia glabra oil based polyesteramide," *Progress in Organic Coatings*, vol. 69, no. 4, pp. 517–521, 2010.

[20] M. Y. Shah and S. Ahmad, "Waterborne vegetable oil epoxy coatings: preparation and characterization," *Progress in Organic Coatings*, vol. 75, no. 3, pp. 248–252, 2012.

[21] T. O. Siyanbola, K. Sasidhar, B. Anjaneyulu et al., "Antimicrobial and anti-corrosive poly (ester amide urethane) siloxane modified ZnO hybrid coatings from *Thevetia peruviana* seed oil," *Journal of Materials Science*, vol. 48, no. 23, pp. 8215–8227, 2013.

[22] A. Chaudhari, A. Kuwar, P. Mahulikar, D. Hundiwale, R. Kulkarni, and V. Gite, "Development of anticorrosive two pack polyurethane coatings based on modified fatty amide of Azadirachta indica Juss oil cured at room temperature-a sustainable resource," *RSC Advances*, vol. 4, no. 34, pp. 17866–17872, 2014.

[23] S. Dutta, N. Karak, and S. Baruah, "Jute-fiber-reinforced polyurethane green composites based on Mesua Ferrea L. Seed oil," *Journal of Applied Polymer Science*, vol. 115, no. 2, pp. 843–850, 2010.

[24] L. Maisonneuve, T. Lebarbé, E. Grau, and H. Cramail, "Structure-properties relationship of fatty acid-based thermoplastics as synthetic polymer mimics," *Polymer Chemistry*, vol. 4, no. 22, pp. 5472–5517, 2013.

[25] R. Müller and G. Wilke, "Synthesis and radiation curing of acrylated castor oil glycerides," *Journal of Coatings Technology Research*, vol. 11, no. 6, pp. 873–882, 2014.

[26] P. D. Meshram, R. G. Puri, A. L. Patil, and V. V. Gite, "High performance moisture cured poly(ether-urethane) amide coatings based on renewable resource (cottonseed oil)," *Journal of Coatings Technology Research*, vol. 10, no. 3, pp. 331–338, 2013.

[27] M. Kashif, F. Zafar, and S. Ahmad, "Pongamia glabra seed oil based poly(urethane-fatty amide)," *Journal of Applied Polymer Science*, vol. 117, no. 3, pp. 1245–1251, 2010.

[28] A. A. Gürten, H. Keleş, E. Bayol, and F. Kandemirli, "The effect of temperature and concentration on the inhibition of acid corrosion of carbon steel by newly synthesized Schiff base," *Journal of Industrial and Engineering Chemistry*, vol. 27, pp. 68–78, 2015.

[29] S. Waśkiewicz, K. Zenkner, E. Langer, M. Lenartowicz, and I. Gajlewicz, "Organic coatings based on new Schiff base epoxy resins," *Progress in Organic Coatings*, vol. 76, no. 7-8, pp. 1040–1045, 2013.

[30] T. Ahamad and S. M. Alshehri, "Thermal, microbial, and corrosion resistant metal-containing poly(Schiff) epoxy coatings," *Journal of Coatings Technology Research*, vol. 9, no. 5, pp. 515–523, 2012.

[31] E. Langer, S. Waśkiewicz, H. Kuczyńska, and G. Kamińska-Bach, "Self-stratifying coatings based on Schiff base epoxy resins," *Journal of Coatings Technology Research*, vol. 11, no. 6, pp. 865–872, 2014.

[32] S. M. Alshehri and T. Ahamad, "New thermal and microbial resistant metal-containing epoxy polymers," *Bioinorganic Chemistry and Applications*, vol. 2010, Article ID 976901, 7 pages, 2010.

[33] E. Sharmin, S. M. Ashraf, and S. Ahmad, "Synthesis, characterization, antibacterial and corrosion protective properties of epoxies, epoxy-polyols and epoxy-polyurethane coatings from linseed and *Pongamia glabra* seed oils," *International Journal of Biological Macromolecules*, vol. 40, no. 5, pp. 407–422, 2007.

[34] S. Ahmad, S. M. Ashraf, F. Naqvi, S. Yadav, and A. Hasnat, "A polyesteramide from *Pongamia glabra* oil for biologically safe anticorrosive coating," *Progress in Organic Coatings*, vol. 47, no. 2, pp. 95–102, 2003.

[35] B. S. Furniss, A. J. Hannaford, P. W. G. Smith, and A. R. Tatchell, *Vogel's Text Book of Practical Organic Chemistry*, Longman Scientific & Technical, Longman Group UK Limited, 5th edition, 1989.

[36] F. Li, G.-X. Li, J. Zeng, and G.-H. Gao, "Molybdate-doped copolymer coatings for corrosion prevention of stainless steel," *Journal of Applied Polymer Science*, vol. 131, no. 16, Article ID 40602, 2014.

[37] S. K. Dhoke, T. J. M. Sinha, P. Dutta, and A. S. Khanna, "Formulation and performance study of low molecular weight, alkyd-based waterborne anticorrosive coating on mild steel," *Progress in Organic Coatings*, vol. 62, no. 2, pp. 183–192, 2008.